Influence of the ZnO buffer on the guided mode structure in Si/ZnO/Ag multilayers

F.-J. Haug,[a] T. Söderström, O. Cubero, V. Terrazzoni-Daudrix, and C. Ballif
Photovoltaics and Thin Film Electronics Laboratory, Institute of Microengineering (IMT), École Polytechnique Fédérale de Lausanne (EPFL), Rue A.-L. Breguet 2, CH-2000 Neuchâtel, Switzerland

(Received 4 May 2009; accepted 14 July 2009; published online 19 August 2009)

We present a study of the optical mode structure in metal-dielectric multilayer structures that represent amorphous silicon thin film solar cells with metallic back contact. Knowledge of the modal structure represents a first step toward describing absorption enhancement by the interface texture in solar cells. We present a method for determining experimentally the dispersion relations of multilayer films by coupling polarized light in a spectral reflection measurement to eigenmodes, using a one-dimensional sinusoidal grating. Because the used grating represents only a minor perturbation that establishes the coupling, the experimental data is well explained by the modal structure of a geometry with flat interfaces. On the basis of the measured mode structure, we propose an explanation for the beneficial effect of a low index buffer layer between the silicon absorber and the metallic back reflector. © *2009 American Institute of Physics*.
[DOI: 10.1063/1.3203937]

I. INTRODUCTION

Thin film solar cells based on amorphous or microcrystalline silicon have become an attractive alternative to their counterparts produced from wafers based single- or multicrystalline material. In order to increase their market share, the current development aims at lower production cost and higher throughput by further reducing the thickness of the absorbing silicon layers. For amorphous solar cells this approach has the additional benefit that thinner cells exhibit less light induced degradation.[1]

In order to keep a high level of photocurrent, thin devices require advanced light management schemes. In most of the state-of-the-art devices, the optical path of incident radiation is enhanced by scattering at interface textures.[2] For example, when aluminum or silver are grown at high temperatures, crystallization of the growing film can develop natural surface structures which are well suited as growth template for subsequent layers.[3,4] Alternatively, transparent conducting oxides such as fluorine doped tin oxide (SnO_2:F) or ZnO also develop surface texture during growth[5,6] or in subsequent etching steps.[7,8] Common to the random structures is a relatively poor control on size and shape of the structures because they are often given by, or related to, the evolution of preferential surface facets. Solar cells with controlled surface texture such as periodic gratings have been proposed at the same time as random structures,[9] but engineered structures on large areas and at low cost have become available only rather recently; using a periodically textured plastic substrate that had been manufactured in a large area roll-to-roll embossing process, we were able to show excellent light trapping in flexible thin film silicon solar cells.[10,11]

Owing to the dominance of random structures, the description of light absorption in thin film silicon solar cells typically assumes scattering at randomly rough surfaces based on scalar scattering theory.[12] Within the films, the propagation of plane waves is assumed.[13,14] In this context, a simplified understanding of light trapping assumes that rays bounce back and forth within the high index absorber layer because of total internal reflection at layers with lower refractive index. This geometrical concept is also quite common for the understanding of waveguides. In both cases, surface corrugations are used for coupling between radiation and the active layers. Owing to the reversibility of the light path, textures can mediate in- as well as outcoupling. In this investigation we propose to take the analogy further; we would like to describe absorption enhancement in the solar cell by the excitation of waveguide modes (eigenmodes) and their attenuated propagation within the multilayer structure. We present measurements of the eigenmode structure of solar cell stacks with different back reflectors for *s*- and *p*-polarization, and we relate the results to the theoretical mode structure using realistic values of the refractive indices.

II. EXPERIMENTAL

Measurements of the dispersion relation are carried out by grating coupling between incident light and propagating modes in the multilayer structure.[15] The grating used in this investigation is a one-dimensional (1D) sinusoidal line grating with a period of 890 nm and an amplitude of 70 nm (half the peak to valley depth) embossed into the surface of a polyethylene substrate supplied by OVD Kinegram AG, Switzerland. We are using similarly embossed substrates by the same supplier for the development of fully flexible thin film silicon solar cells.[10,11,16] The grating is covered with back reflector structures consisting of 90 nm Ag and Ag covered with ZnO of three different thicknesses (20, 40, and 60 nm). The Ag is deposited in a multisource sputtering system by dc sputtering (Univex 450B, Leybold). The ZnO films are deposited in the same system without vacuum break, but by rf sputtering from a ceramic ZnO target that contains 2 wt %

[a]Electronic mail: franz-josef.haug@epfl.ch.

Al_2O_3. Oxygen is added during the deposition of ZnO in order to obtain high transparency and to reduce the impact of free carrier absorption in the IR. The resulting films are highly resistive; we obtain 2–3 Ω cm in reference depositions on glass. The amorphous silicon was grown by plasma enhanced chemical vapor deposition using at 70 MHz (VHF) at a substrate temperature of 190 °C using a silane-hydrogen mixture with a dilution $[H_2]/[SiH_4]$ equal to two. The silicon films used in this investigation have a thickness of 200 nm. The measurement of total reflection was carried out with a spectrometer with integrating sphere (PerkinElmer, Lambda 900). The reflection port of this system is tilted by 7° with respect to the incident beam. For measurements with polarized light, a broad band wire polarizer (ProFlux PPL05C, Moxtek) was installed in the spectrometer before the baseline measurement. The relation between the tilt and the polarization directions will be discussed in Sec. III. IR reflection measurements without polarization have been done with a FTIR spectrometer (Nicolet 8700, Thermo)

III. THEORY

The layer sequence of the thin film solar cell can be regarded as slab waveguide in a somewhat unusual configuration; the silicon absorber layer corresponds to the active waveguide layer, the metallic back contact represents the cladding layer. The ZnO layer acts as low index spacer between cladding and waveguide. In the following, we briefly define the notation and sketch some concepts of the flat planar waveguide terminology that apply to our configuration.

A. Fresnel equations

Resonances of an optical system are easily identified by poles of the corresponding Fresnel reflection coefficient (see, e.g., Appendix II in Ref. 17); for a single interface the reflection coefficients are given by

$$r_{12} = \frac{S_1 - S_2}{S_1 + S_2} \quad (s\text{-polarization}), \tag{1}$$

$$r_{12} = \frac{\varepsilon_2 S_1 - \varepsilon_1 S_2}{\varepsilon_2 S_1 + \varepsilon_1 S_2} \quad (p\text{-polarization}). \tag{2}$$

The quantity S_i is defined in each layer by $S_i^2 = k^2 - \varepsilon_i k_\parallel^2$, using the complex dielectric function $\varepsilon = \varepsilon' + i\varepsilon''$ of each individual layer, and $k_\parallel$ is the in-plane component of the free space wave vector $k_\parallel = 2\pi/\lambda \cdot \sin\theta$. We solve for k values at given incident photon energy $\hbar\omega$; k represents the wave vector of a mode that propagates parallel to the interface. In general k is a complex functions of ω, thus $k = k' + ik''$, and the imaginary part k'' denotes the attenuation of the propagation in the in-plane direction. Often a dimensionless propagation constant β is defined by normalizing the solution k to the value of the free space wave vector

$$\beta = \beta' + i\beta'' = \frac{k}{k_0} = \frac{k}{2\pi/\lambda}.$$

B. Surface plasmon resonance

The condition of poles in Eqs. (1) and (2) (i.e., zero denominator) cannot be met for *s*-polarization. For *p*-polarization it can be met, and an analytical solution is possible whenever the real part of ε_2 is negative and the condition $|\varepsilon_2| > \varepsilon_1$ is fulfilled; this is possible for the combination of a dielectric and a metal. By eliminating S_1 and S_2, we obtain a relation for $k(\omega)$,

$$k(\omega) = \pm \frac{\omega}{c}\left(\frac{\varepsilon_1\varepsilon_2}{\varepsilon_1 + \varepsilon_2}\right)^{1/2}. \tag{3}$$

The Eq. (3) represents the dispersion relation of the well known surface plasmon polariton (SPP) first described by Ritchie.[18] In the out-of-plane direction, the amplitude of the electric field of the SPP assumes a maximum value at the interface and decays exponentially into the two adjacent media.

Frequently Eq. (3) is evaluated using only the real parts of the dielectric functions ε_1' and ε_2', and the result is taken as approximation for the real part of the wave vector k'. Typically, this approximation is valid when $|\varepsilon'_{\text{metal}}| \gg \varepsilon''_{\text{metal}}$, e.g., for silver in the visible and IR range. In the same range of validity, the imaginary part k'' of the SPP is approximated by[17]

$$k''(\omega) = \frac{\omega}{c}\frac{\varepsilon_2''(\omega)}{2[\varepsilon_2'(\omega)]^2}\left[\frac{\varepsilon_1\varepsilon_2'(\omega)}{\varepsilon_1 + \varepsilon_2'(\omega)}\right]^{3/2}. \tag{4}$$

In this paper, the single interface approximations of Eq. (3) or (4) are included in several figures for the illustration of limiting behavior; in this contribution they are plotted with full lines if not specified differently.

C. Grating coupling

The term in the square root of Eq. (3) is always larger than one, thus the dispersion relation never intersects with the dispersion relation of a photon which is given by $k(\omega) = \omega/c$. A direct excitation of SPPs by light incident from air or vacuum is therefore not possible on a flat metal surface because energy and momentum must be conserved. Surface corrugations, in particular gratings, can mediate the coupling by relaxing the conservation of the momentum. As long as the surface corrugations can be treated as small perturbation of the flat surface, we can continue to consider eigenmodes of the flat case and assume that the grating only acts as coupling for the excitation of resonances. At given energy, small perturbations generally shift the real part k' to slightly higher values while the imaginary part can increase by orders of magnitude due to so-called radiation damping.[17] In the presence of periodic surface corrugations the considerations become particularly easy; the photon can pick up or loose momentum in multiples of the reciprocal lattice vector, which corresponds to a translation into an adjacent Brillouin zone

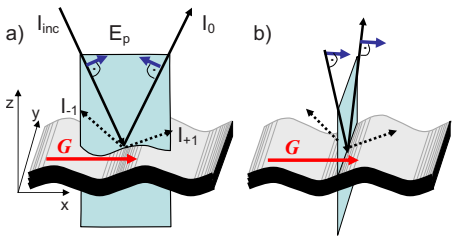

FIG. 1. (Color online) Drawing (a) illustrates the commonly used definition of polarization directions; in *p*-polarization the E-field is contained within the plane that is spanned by the incident and reflected beam ("parallel"). Correspondingly, the E-field of *s*-polarization is perpendicular ("senkrecht") to this plane. The rotated configuration of drawing (b) was used in this study; with respect to the grating this represents a conical mount.

$$k_{\parallel} = k_0 \sin\theta + m \cdot \frac{2\pi}{L}, \quad m = \pm 1, \pm 2, \pm 3, \ldots . \tag{5}$$

In Eq. (5), $k_{\parallel}$ is the in-plane component of the wave vector, k_0 is the wave vector value of the photon in vacuum, θ is the angle of incidence with respect to the surface normal, L is the period of the grating, and m is an integer.

D. Measurement geometry

The excitation of SPPs is commonly investigated with *p*-polarized light in the configuration of Fig. 1(a); in this case, the E-field is contained in the plane that is spanned by the incident and the reflected beams. When either the wavelength or the angle of incidence is increased, the diffracted orders are excited into larger angles and eventually become evanescent. Due to grating coupling, the +1 diffraction order is coupled to a forward traveling SPP (parallel to G). Likewise, at yet longer wavelength or reduced angle of incidence, the -1 order becomes evanescent and couples to a backward traveling SPP (antiparallel to G). The frequent use of this measurement geometry leads to the notion that SPPs are excited only by *p*-polarized light. However, the decisive condition for the excitation of SPPs is related to the orientation of the E-field with respect to the grating vector G; keeping the polarizer in place and changing to the conical mount illustrated in Fig. 1(b), SPPs are still excited by the diffracted beams, even though the configuration now represents *s*-polarization according to the definition in terms of incident and diffracted beams.

We use the conical mount throughout this investigation because the wave vector of the incident light is then perpendicular to the reciprocal lattice vector G. Thus, interactions are translated simply into the centers of the higher order Brillouin zones because the first term on the right hand side of Eq. (5) is zero. In other words, forward and backward propagating SPPs become degenerate. This procedure facilitates the interpretation of reflection spectra like the one shown in Fig. 2 because fewer absorptions with higher amplitude are measured. In order to be consistent with the bulk of literature on SPPs and waveguides, we will refer to *p*-polarization whenever SPPs can be excited, including the geometry of Fig. 1(b).

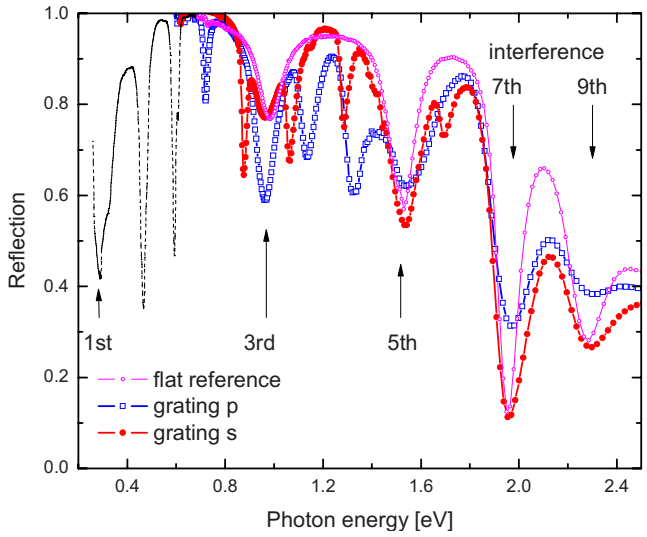

FIG. 2. (Color online) Spectral reflection of 200 nm thick silicon films on silver on a flat reference substrate and on the 1D grating. The periodic structure mediates the excitation of a variety of eigenmodes for each of the two polarization directions (the measurement in the near IR has been performed with unpolarized light).

E. Guided modes

In systems with two interfaces between three media, the Fresnel coefficient r_{123} is defined in terms of the individual reflection coefficients of the single interfaces by Eqs. (1) and (2) for *s*- and *p*-polarization, respectively, and an exponential term that takes care of propagation within the film of thickness d_2

$$r_{123} = \frac{r_{12} + r_{23}\exp\{-2S_2 d_2\}}{1 + r_{12}\cdot r_{23}\exp\{-2S_2 d_2\}}. \tag{6}$$

The condition of zero denominator in Eq. (6) yields relations for a wide range of phenomena; the three layer stack is the most simple geometry that allows resonances for *s*-polarization, and a well studied configuration is the dielectric waveguide that consists of a high index guiding layer embedded into materials with lower index.[19,20] With varying thickness of the high index layer, the periodicity of the exponential in the denominator of Eq. (6) gives rise to a multitude of modes. These are called guided modes because their propagation is parallel to the interfaces such as SPPs, but their electromagnetic field resides mostly within the dielectric.

The resonances condition in Eq. (6) using *p*-polarization and a thin metallic film on a substrate can be used to describe the coupling between the SPPs on the two interfaces. Their splitting into two branches of short and long range has been proposed for subwavelength signal transmission.[21–23] Using *p*-polarization and a thin dielectric film on semi-infinite metal, the solutions are similar to the case of to the already discussed SPPs. With increasing thickness of the dielectric film there is again a multitude of guided modes.[24] In fact, the SPP represents the zero order TM guided mode waveguide terminology because the normal component of the electric field has no nodes.

For our experimental geometry with a thin ZnO layer between the silicon absorber layer and the silver back reflec-

tor we need to consider the Fresnel coefficients of the four layer system consisting of air (semi-infinite, $\varepsilon_1=1$), silicon with dielectric constant ε_2 and thickness d_2 (fixed to 200 nm in this study), ZnO with dielectric constant ε_3 and thickness d_3, and silver with the dielectric function ε_4 (note that the thickness of 90 nm used in this investigation justifies to treat the metal layer as semi-infinite substrate, see Ref. 15). The optical properties of the system are obtained from the four layer Fresnel reflection coefficient which is recursively defined in terms of the three layer coefficient of Eq. (6).

$$r_{1234} = \frac{r_{12} + r_{234}\exp\{-2S_2d_2\}}{1 + r_{12} + r_{234}\exp\{-2S_2d_2\}} = \frac{r_{12} + \dfrac{r_{23} + r_{34}\exp\{-2S_3d_3\}}{1 + r_{23}r_{34}\exp\{-2S_3d_3\}}\exp\{-2S_2d_2\}}{1 + r_{12} + \dfrac{r_{23} + r_{34}\exp\{-2S_3d_3\}}{1 + r_{23}r_{34}\exp\{-2S_3d_3\}}\exp\{-2S_2d_2\}}. \quad (7)$$

The four layer system has frequently been used for the investigations of resonances in attenuated total reflection configuration, taking explicitly into account the coupling prism (medium 1), the air gap (medium 2 with thickness d_2), a thin film (medium 3 with finite thickness d_3), and the substrate (medium 4).[25–27]

IV. EXPERIMENTAL RESULTS

Figure 2 shows the spectral reflection of a 200 nm thick film of amorphous silicon directly on the silver covered grating (without ZnO). On the flat reference, the reflection shows a series of interference dips which are indexed with their respective orders. On the grating, there are additional absorption dips at distinct energies for the two possible directions of polarization. Similar spectra have been measured on samples where ZnO layers of varying thickness have been inserted between the silver and the silicon.

The grating mediated dips (i.e., all except the interferences) have been related to the coordinates of a dispersion diagram in the form of $\omega=\omega(k)$ by applying the condition of grating coupling and perpendicular incidence according to Eq. (5). There is some ambiguity at low and at high energies; in the IR range we did not have access to a polarized measurement but the spectrometer data in Fig. 2 show the onset of an absorption dip in *s*-polarization; thus, we attribute the low and high energy dips above the interference minimum in the IR data as *p*- and *s*-polarized, respectively. In the high energy range the spectrometer measurement does resolve the polarization dependence, but the coupling with a low order mode in a high order Brillouin zone can occur in an energy range where there is also coupling to a high order mode in a lower order zone. In most cases a unique attribution was possible by looking at systematic changes within the ZnO thickness series.

The experimentally determined dispersion relations of our sample set are summarized in Fig. 3. Figure 4 presents corresponding numerical solutions obtained by demanding the denominator of Eq. (7) to become zero. The lowest energy interactions are due to the zero order *p*-polarized

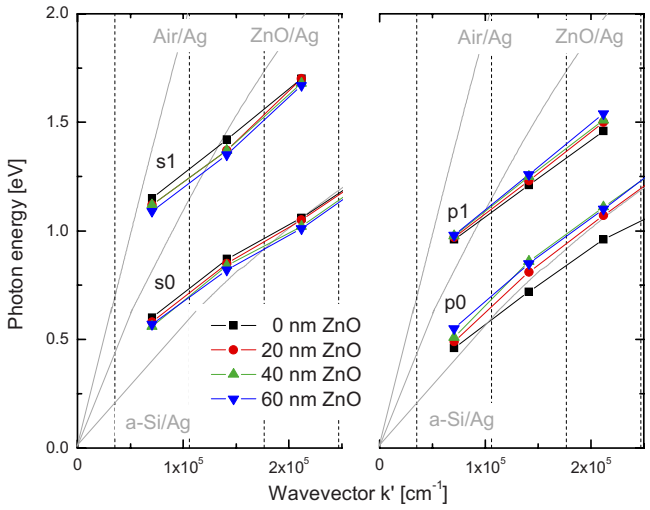

FIG. 3. (Color online) Measured dispersion relations $\omega(k)$ of surface plasmon and guided modes in Si/ZnO/Ag structures. The symbol type represents the ZnO thickness variation between 0 and 60 nm; the left panel shows *s*-polarization and the right panel shows *p*-polarization. The curves emerging from the origin illustrate the theoretical dispersion relations of the plasmon resonance at the interfaces between silver and air, zinc oxide, and silicon, respectively, and the vertical dashed lines represent Brillouin zone boundaries.

modes. A comparison with Fig. 4 shows that they appear at lower energies than theoretically expected. The relatively large difference to the theoretical prediction of the *p*0 modes is probably related to fact that the periodic surface structure of our experimental setup represents a perturbation to the flat interface that we used for the calculation. The zero order *p*-modes of samples with the ZnO buffer layer show that increasing ZnO thickness shifts the dispersion relations upwards rapidly.

At higher energy, *s*-polarized guided modes of zero order appear; a comparison of Figs. 3 and 4 reveals that in this case the position of the interactions agree well with the flat surface model. Because of the upward shift of the *p*-modes and

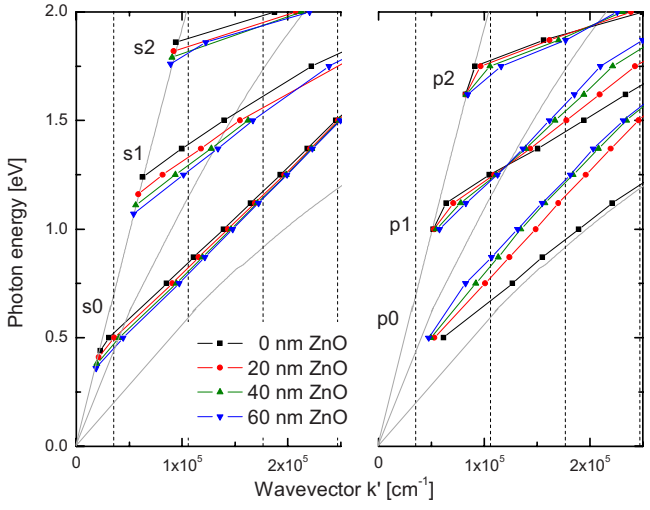

FIG. 4. (Color online) Calculated dispersion relations $\omega(k)$ for the configurations shown in Fig. 3, using the same symbol types and scale. Different from the measurement on the sinusoidal grating, the flat interface model predicts higher energies for all *p*0 modes.

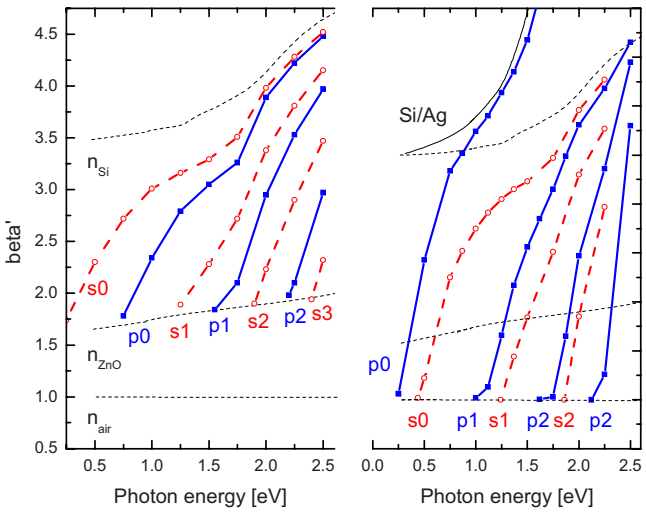

FIG. 5. (Color online) Comparison of the modal structure $\beta'(\omega)$ calculated for three layer structures consisting of air/Si/ZnO (left) and air/Si/Ag (right). The *s*- and *p*-polarizations are denoted by open circles and full squares, respectively. Thin dashed lines denote the refractive indices of the respective materials. The solid line in the upper part of the right panel shows the dispersion relation of the SPP at the Si/Ag interface (normalized to the vacuum wave vector value k_0).

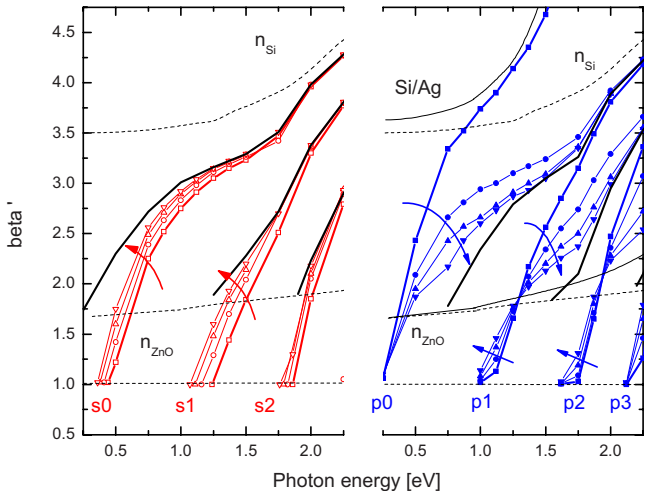

FIG. 6. (Color online) Real part $\beta'(\omega)$ of the dispersion relation of *s*-polarized (left panel) and *p*-polarized modes (right panel), normalized to the vacuum wave vector k_0. Squares, circles up and down triangles denote the thickness variation of ZnO between 0, 20, 40, and 60 nm, the dashed lines represent the refractive indices of the different media (air, ZnO and silicon), the thin full lines represent the normalized plasmon dispersion relations of the Si/Ag and the ZnO/Ag interfaces according to Eq. (3). Thick full lines show the modes of an air/Si/ZnO three layer waveguide from Fig. 5.

the downward shift of the *s*-modes, there is a crossing of the *p*- and the *s*-mode characteristics for ZnO thickness between 40 and 60 nm.

At yet higher energies, we find interactions that we attribute to first order guided modes of *p*-polarization, and then *s*-polarization. While their signatures were relatively weak in the reflection data, their measured energies correspond better with the prediction of the model. Higher order guided modes which are predicted to appear at about 1.75 eV have not been observed because an interference dip and the onset of absorption in Si overlap in that region (cf. Fig. 2). Apart from the low energy deviations we find a general agreement between Figs. 3 and 4, indicating that the use of the flat surface model yields a qualitative description of the waveguide modes in the solar cell stack on the grating.

V. DISCUSSION

For the discussion of the observations we consider the limiting behavior of our samples by using the three layer case of Eq. (6) considering a 200 nm thick film of amorphous silicon limited by air on one side (no front contact) and either ZnO or silver as semi-infinite bulk substrates. Figure 5 shows a normalized plot of $\beta'(\omega)$; the air/Si/ZnO structure clearly reveals the modal structure of an asymmetric dielectric waveguide in a planar geometry where a high index material (amorphous silicon) is embedded between two materials with lower but different indices (air and the semi-infinite ZnO substrate). The lowest energy mode is the zero order *s*-polarized wave (*s*0), followed by the zero order mode of *p*-polarization (*p*0). With increasing energy, higher order modes of *s*- and *p*-polarization appear alternatingly. All modes show a transition from a low energy onset ("cutoff") starting from the higher of the two adjacent low refractive indices (ZnO) toward the index of the guiding medium (silicon). This behavior explains why the quantity β' is also called effective refractive index of the guided wave. Typical for asymmetric waveguides, there is a low energy cutoff energy for the *s*0 mode, below which no guided mode is supported in the structure (cutoff at about 0.2 eV, not shown in the diagram).

The modal structure of the air/Si/Ag shown in the right panel in Fig. 5 reveals that in this case the lowest energy mode is *p*-polarized. All modes start at a low energy limit corresponding to the refractive index of air. Toward high energies, the *p*0 mode approaches the characteristic of the SPP of the two layer interface between silicon and silver according to Eq. (3). All higher order *p*-modes show the typical behavior of guided modes.[24,28] Different from the dielectric waveguide, however, the *p*-mode of a given order is always lower in energy than the *s*-mode.

The effect of the ZnO layer between silicon and silver is different for the two polarization directions. The left panel in Fig. 6 shows that *s*-modes change toward larger values of β'. Within the different orders, the effect is quite pronounced around the onset but becomes weaker toward high energies. The behavior of the *p*-modes in the right panel is more complicated; in the lower part close to onset they also show the behavior of increasing β', similar to the *s*-modes. However, we find that the dispersion relation of the SPP at the ZnO/Ag interface marks a transition to a different behavior; above this curve, the introduction of the ZnO layer actually reduces the value of β'. The limiting behavior is defined by the asymmetric air/Si/ZnO three layer waveguide which was already shown in Fig. 5. The ZnO layer thus effectively establishes a situation like in a "standard" dielectric waveguide where *s*-modes are the lowest energy modes and *p*-modes follow at higher energy. This is an important conclusion for the application as back contact in solar cells; the ZnO layer prohibits the existence of the SPP mode with its high field

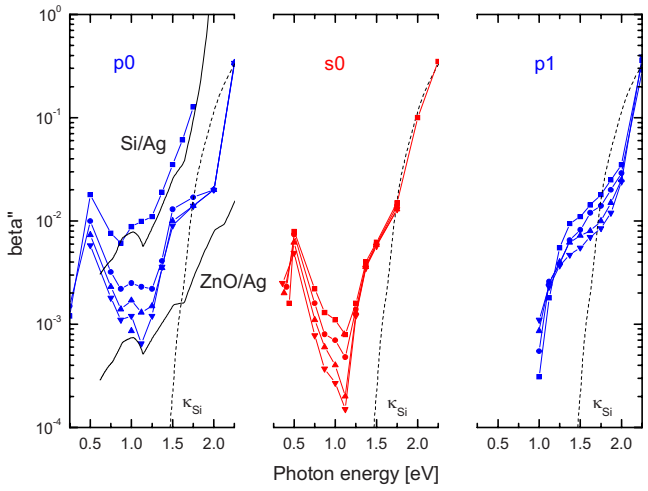

FIG. 7. (Color online) Imaginary part $\beta''(\omega)$ of the lowest order guided modes in Fig. 6. The dashed line represents the extinction coefficient of silicon (κ_{Si}) and the full lines in the left panel denote the normalized attenuation of the plasmon dispersion relations of the Si/Ag and the ZnO/Ag interfaces according to Eq. (4). Squares, circles, up and down triangles correspond to ZnO thickness of 0, 20, 40, and 60 nm, respectively.

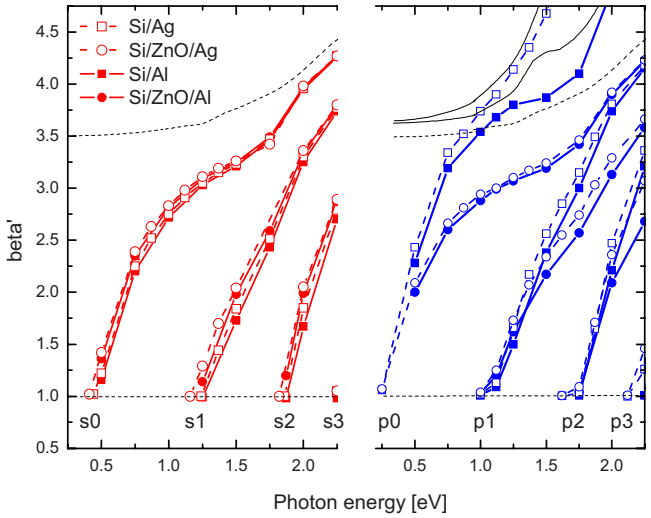

FIG. 8. (Color online) Comparison of the mode structure in silicon on silver (open symbols and dashed lines) and aluminum back reflectors (full symbols and full lines). The Si/metal interface is denoted by squares and circles represent a 20 nm ZnO buffer layer.

intensity at the metal surface, and it converts the low energy $p0$ mode into a guided wave with maximum field intensity within the high index silicon layer.

Figure 7 shows the imaginary part β'' of the lowest orders. We observe transitional behavior similar to the case of the real part; at low energies, β'' of the $p0$ modes shows a transition between the SPP attenuations according to Eq. (4) for the limiting cases of the Si/Ag and the ZnO/Ag interfaces, respectively, whereas at higher energies the transition is toward the value of the extinction coefficient in silicon. The latter behavior is observed for all guided modes at energies higher than 2 eV and represents the onset of strong absorption in silicon. Note however, that the attenuation is heavily influenced by the surface texture and the results for the flat interface given here serve only as indication of the transitional behavior.

We conclude by extending the model toward aluminum as an alternate back contact material. Figure 8 compares the dispersion relations of silicon on silver and on aluminum (as in previous calculations with silver, we consider a semi-infinite aluminum substrate). The figure includes the case where a ZnO buffer layer is inserted, but for clarity we show only one single ZnO thickness of 20 nm. The s-modes show very little sensitivity toward the back contact metal or the presence or absence of the buffer layer. The most important differences are noted for the SPPs ($p0$ modes) of the interfaces without ZnO buffer layer; this mode most sensitively probes the differences in the dielectric functions of the two metals. Indeed, in case of aluminum there is also an indication that the approximation of Eq. (3) differs significantly from the more precise numerical solution which is denoted by the symbols. After insertion of the buffer layer, however, the $p0$ mode is much less sensitive toward the back contact metal, again highlighting the beneficial effect of the buffer layer. The behavior of higher order p-modes varies; the $p1$ modes depend only marginally on the metal, but they do show strong changes after the introduction of the buffer. In contrast, among the $p2$ modes only the configuration with ZnO on aluminum shows a different behavior above 2.2 eV. Finally, we note that the attenuations curves shown in Fig. 9 are at least one order of magnitude higher whenever aluminum is used as back reflector metal. We take this as an indication that more parasitic absorption takes place in the back reflector metal.

VI. CONCLUSIONS

We presented an experimental determination of the optical eigenmode structure of a multilayer solar cell stack incorporating a layer of thin film silicon and different back reflector scenarios. We find that a dielectric buffer layer between the amorphous silicon absorber and the metal back contact converts the p-polarized zero order mode from the excitation of a surface plasmon resonance localized at the metallic interface into a regular waveguide mode whose field

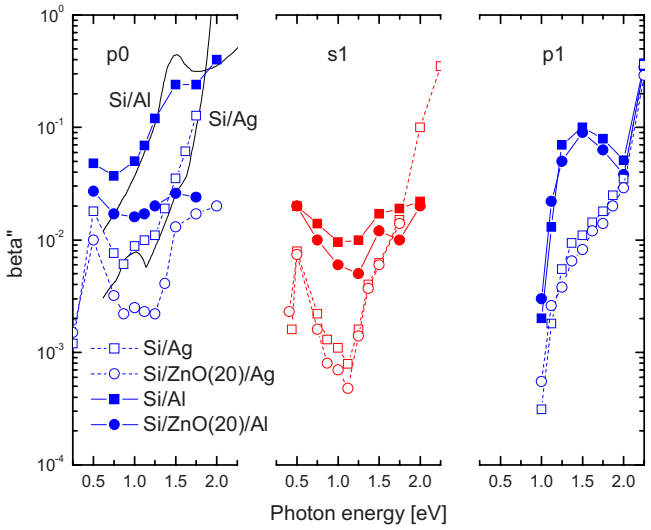

FIG. 9. (Color online) Imaginary part $\beta''(\omega)$ of the lowest order modes on Ag and Al reflectors (line styles such as Fig. 8).

intensity is located mainly in the silicon film. Thus, parasitic absorption in the metal film is reduced and a more favorable situation is established where absorption takes place in the silicon layer. We extend the considerations to the technologically important case of aluminum reflectors where the insertion of ZnO converts the modal structure again toward a more favorable case of mode guiding within the silicon absorber layer.

ACKNOWLEDGMENTS

We thankfully acknowledge funding within the European Project "Flexcellence" under Contract No. 019948 and from the Swiss Federal Office of Energy in Project No. 101191.

[1]J. J. Hanak and V. Korsun, Proceedings of the 16th IEEE PVSC, San Diego, 1982 (unpublished), pp. 1381–1383.
[2]H. W. Deckman, C. R. Wronski, H. Witzke, and E. Yablonovitch, Appl. Phys. Lett. **42**, 968 (1983).
[3]M. Hirasaka, K. Suzuki, K. Nakatani, M. Asano, M. Yano, and H. Okaniwa, Sol. Energy Mater. **20**, 99 (1990).
[4]A. Banerjee and S. Guha, J. Appl. Phys. **69**, 1030 (1991).
[5]M. Kambe, M. Fukawa, N. Taneda, Y. Yoshikawa, K. Sato, K. Ohki, S. Hiza, A. Yamada, and M. Konagai, Proceedings of the Third World PVSEC, Osaka, 2003 (unpublished), pp. 1812–1815.
[6]S. Fay, J. Steinhauser, N. Oliveira, E. Vallat-Sauvain, and C. Ballif, Thin Solid Films **515**, 8558 (2007).
[7]O. Kluth, B. Rech, L. Houben, S. Wieder, G. Schöpe, C. Beneking, H. Wagner, A. Löffl, and H. W. Schock, Thin Solid Films **351**, 247 (1999).
[8]J. Bailat, D. Dominé, R. Schlüchter, J. Steinhauser, S. Faÿ, F. Freitas, C. Bücher, L. Feitknecht, X. Niquille, R. Tscharner, A. Shah, and C. Ballif, Proceedings of the Fourth World PVSEC, Hawaii, 2006 (unpublished), pp. 1533–1536.
[9]P. Sheng, A. N. Bloch, and R. S. Stepleman, Appl. Phys. Lett. **43**, 579 (1983).
[10]F.-J. Haug, T. Söderström, M. Python, V. Terrazzoni-Daudrix, X. Niquille, and C. Ballif, Sol. Energy Mater. Sol. Cells **93**, 884 (2009).
[11]T. Söderström, F. J. Haug, X. Niquille, V. Terrazoni-Daudrix, and C. Ballif, Appl. Phys. Lett. **94**, 063501 (2009).
[12]H. E. Bennett and J. O. Porteus, J. Opt. Soc. Am. **51**, 123 (1961).
[13]A. Poruba, A. Fejfar, Z. Remeš, J. Špringer, M. Vanecek, J. Kocka, J. Meier, P. Torres, and A. Shah, J. Appl. Phys. **88**, 148 (2000).
[14]J. Krc, F. Smole, and M. Topic, Prog. Photovoltaics **11**, 15 (2003).
[15]F.-J. Haug, T. Söderström, O. Cubero, V. Terrazzoni-Daudrix, and C. Ballif, J. Appl. Phys. **104**, 064509 (2008).
[16]J. Bailat, V. Terrazzoni-Daudrix, J. Guillet, F. Freitas, X. Niquille, A. Shah, C. Ballif, T. Scharf, R. Morf, A. Hansen, D. Fischer, Y. Ziegler, and A. Closset, Proceedings of the 20th European PVSEC, Barcelona, 2005 (unpublished).
[17]H. Raether, *Surface Plasmons*, Springer Tracts on Modern Physics Vol. 111 (Springer, New York, 1988).
[18]R. H. Ritchie, Phys. Rev. **106**, 874 (1957).
[19]D. Nelson and J. McKenna, J. Appl. Phys. **38**, 4057 (1967).
[20]S. Yamamoto, Y. Koyamada, and T. Makimoto, J. Appl. Phys. **43**, 5090 (1972).
[21]D. Sarid, Phys. Rev. Lett. **47**, 1927 (1981).
[22]T. Inagaki, M. Motosuga, E. T. Arakawa, and J. P. Goudonnet, Phys. Rev. B **32**, 6238 (1985).
[23]J. J. Burke, G. I. Stegeman, and T. Tamir, Phys. Rev. B **33**, 5186 (1986).
[24]A. Adams, J. Moreland, P. K. Hansma, and Z. Schlesinger, Phys. Rev. B **25**, 3457 (1982).
[25]P. K. Tien, R. Ulrich, and R. J. Martin, Appl. Phys. Lett. **14**, 291 (1969).
[26]L. Wendler and R. Haupt, Phys. Status Solidi B **143**, 131 (1987).
[27]M. Klopfleisch, M. Golz, and U. Trutschel, Appl. Opt. **31**, 5017 (1992).
[28]I. Pockrand, J. Phys. D **9**, 2423 (1976).